

# We are IntechOpen, the world's leading publisher of Open Access books Built by scientists, for scientists

4,800

Open access books available

122,000

International authors and editors

135M

Downloads

Our authors are among the

154

Countries delivered to

TOP 1%

most cited scientists

12.2%

Contributors from top 500 universities



WEB OF SCIENCE™

Selection of our books indexed in the Book Citation Index  
in Web of Science™ Core Collection (BKCI)

Interested in publishing with us?  
Contact [book.department@intechopen.com](mailto:book.department@intechopen.com)

Numbers displayed above are based on latest data collected.  
For more information visit [www.intechopen.com](http://www.intechopen.com)



# A Computer-assisted Wind Load Evaluation System for the Design of Cladding of Buildings: A Case Study of Spatial Structures

Yasushi Uematsu  
Tohoku University  
Japan

## 1. Introduction

Thin sheet metal and/or membrane are often used for roof cladding of spatial structures because of their strength and lightness (Noguchi et al., 2003). Being light and flexible, such roofing materials are vulnerable to dynamic wind actions. Since wind pressures acting on spatial structures vary spatially as well as in time, the design wind loads should be determined based on the dynamic characteristics of wind pressures. Fatigue of cladding elements, such as roofing material and its fixings, may play an important role in the wind resistant performance of cladding systems, although it is seldom considered in the design.

Roof cladding is usually designed based on the worst peak pressure coefficients irrespective of wind direction. The conventional codification provides a single peak design pressure coefficient for each roof zone considering a nominal worst-case scenario. Neither the probability distribution of the peak pressure coefficients nor the peaks other than the largest one are considered. Hence, they are not suitable for fatigue and risk-consistent designs. Building design has recently shifted to a performance-oriented one. Therefore, it is hoped to develop a new methodology that provides the peak pressure coefficients according to predetermined risk levels and the loading sequence for estimating the fatigue damage to roof cladding and its fixings. Computer simulation of wind pressure time series may be useful for this purpose.

Kumar and Stathopoulos (1998, 1999, 2001) proposed a novel simulating methodology that generates both Gaussian and non-Gaussian wind pressure fluctuations on low building roofs. Despite its simple procedure, the technique is successfully applied to fatigue analysis as well as to the evaluation of extreme pressures in a risk-consistent way. Therefore, this technology is used in this chapter and a simplification of this method is discussed. Gaussian and non-Gaussian pressure fluctuations can be simulated from the statistics of wind pressures, i.e. the mean, standard deviation, skewness, kurtosis and power spectrum. These statistical values change with location as well as with many factors related to the structure's geometry and the turbulence characteristics of approach flow. For such a complicated phenomenon, in which a number of variables involve, artificial neural networks (simply neural networks or ANN's) can be used effectively. Artificial neural networks can capture a complex, non-linear relationship via training with informative input-output example data pairs obtained from computations and/or experiments. Among a variety of artificial neural

networks developed so far, Cascade Correlation Learning Network (Fahlman and Lebiere, 1990) is applied to the present problem. It is a popular supervised learning architecture that dynamically grows layers of hidden neurons of a fixed non-linear activation (e.g. sigmoid), so that the topology (size and depth) can also be efficiently determined.

This chapter proposes a computer-assisted wind load evaluation system for the design of roof cladding of spatial structures. Focus is on spherical domes and vaulted roofs, as typical shapes of spatial structures. The composition of the system is schematically illustrated in Fig. 1. This system provides wind loads for the design of cladding and its fixings without carrying out any additional wind tunnel experiments. An aerodynamic database, artificial neural network and time-series simulation technique are employed in the system. Finally, applications of the system to risk-consistent design as well as to fatigue design are presented.

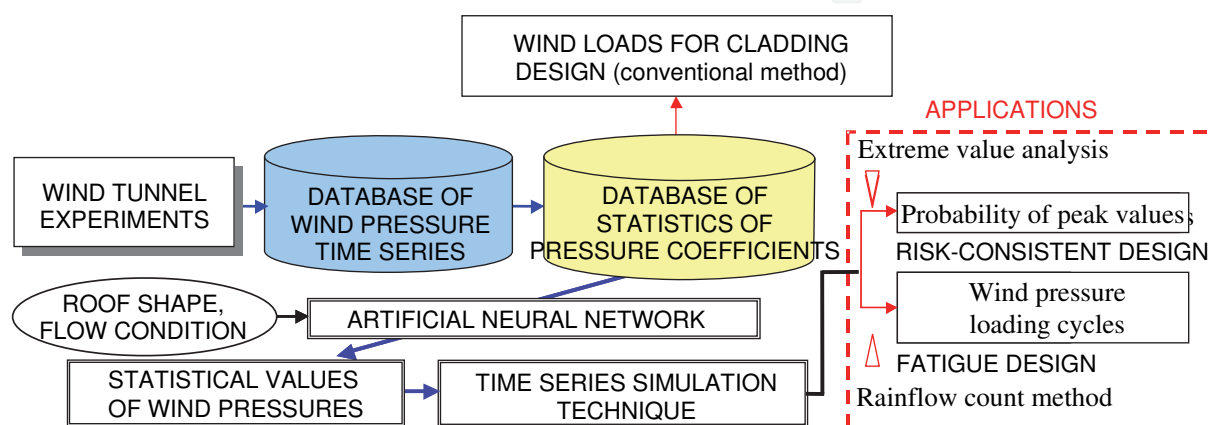


Fig. 1. Wind load evaluation system for the roof cladding of spatial structures

The wind load evaluation system proposed here is based on our previous studies (Uematsu et al., 2005, 2007, 2008). It can be applied not only to spherical domes and vaulted roofs but also to any other structures. However, such a system may be more useful for designing the cladding of spatial structures because of its sensitivity to dynamic load effects of fluctuating wind pressures. The spatial variation of statistical properties and the non-normality of pressure fluctuations on spherical domes and vaulted roofs are less significant than those on flat and gable roofs. Therefore, an ANN and a time-series simulation technique can be used more efficiently for these structures. This is the reason why we focus on the cladding of spherical domes and vaulted roofs in this chapter.

## 2. Aerodynamic database

### 2.1 Wind tunnel experiments

Two series of wind tunnel experiments were carried out; one is for spherical domes and the other is for vaulted roofs. The experimental conditions are somewhat different from each other. The outline of the experimental conditions is presented here.

#### 2.1.1 Spherical dome

The experiments were carried out in a closed-circuit-type wind tunnel with a working section 18.1 m long, 2.5 m wide and 2.0 m high. Two kinds of turbulent boundary layers simulating natural winds over typical open-country and urban terrains were generated; these flows are respectively referred to as Flows 'II' and 'IV' in this chapter. The geometric

scale of these flows ranges from 1/400 to 1/500, judging from the longitudinal integral scale of turbulence.

The geometry of the wind tunnel model is schematically illustrated in Fig. 2(a). The rise/span ratio ( $f/D$ ) is varied from 0 to 0.5, while the eaves-height/span ratio ( $h/D$ ) from 0 to 1. The span  $D$  of the wind tunnel model is 267 mm and the surface of the model is nominally smooth. Each model is equipped with 433 pressure taps of 0.5 mm diameter, as shown in Fig. 2(b). The pressure taps are connected to pressure transducers in parallel via 80 cm lengths of flexible vinyl tubing of 1 mm inside diameter. The compensation for the frequency response of this pneumatic tubing system is carried out by using a digital filter, which is designed so that the dynamic data up to approximately 500 Hz can be obtained without distortion. The signals from the transducers are sampled in parallel at a rate of 1 kHz on each channel for a period of approximately 33 seconds. All measurements are made at a wind velocity of  $U_{ref} = 10$  m/s at a reference height of  $Z_{ref} = 267$  mm. The velocity scale is assumed 1/5. The wind velocity  $U_{top}$  at the level of rooftop ranges from 5.3 to 10.2 m/s; the corresponding Reynolds number  $Re$ , defined in terms of  $D$  and  $U_{top}$ , ranges from approximately  $9.4 \times 10^4$  to  $1.8 \times 10^5$ . The turbulence intensity  $I_{u,top}$  at the level of rooftop ranges from 0.13 to 0.20 for Flow II and from 0.12 to 0.27 for Flow IV.

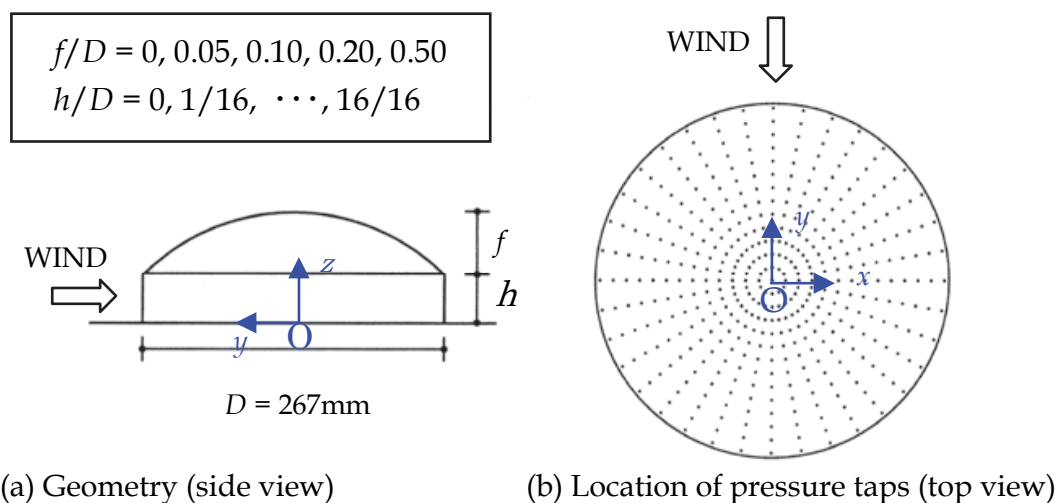


Fig. 2. Wind tunnel model and coordinate system (spherical domes)

### 2.1.2 Vaulted roof

The experiments were carried out in a closed-circuit-type wind tunnel with a working section 18.9 m long, 2.6 m wide and 2.1 to 2.4 m high. Two kinds of turbulent boundary layers similar to those used for spherical domes were generated; these flows are respectively referred to as Flows 'II'' and 'IV'' in this chapter.

The geometry of the wind tunnel model is schematically illustrated in Fig. 3(a). The rise/span ratio ( $f/D$ ) is varied from 0.1 to 0.4, while the eaves-height/span ratio ( $h/D$ ) from 1/30 to 20/30. The span  $D$  of the wind tunnel model is 150 mm and the length  $W$  is 300mm. Each model is equipped with 228 pressure taps of 0.5 mm diameter, as shown in Fig. 3(b). The turbulence intensity  $I_{u,H}$  at the mean roof height  $H$  is approximately 0.16 for Flow II' and approximately 0.19 for Flow IV'.

The experimental procedure is the same as that for spherical domes except that the wind direction is varied from 0 to 90° at a step of 5°.

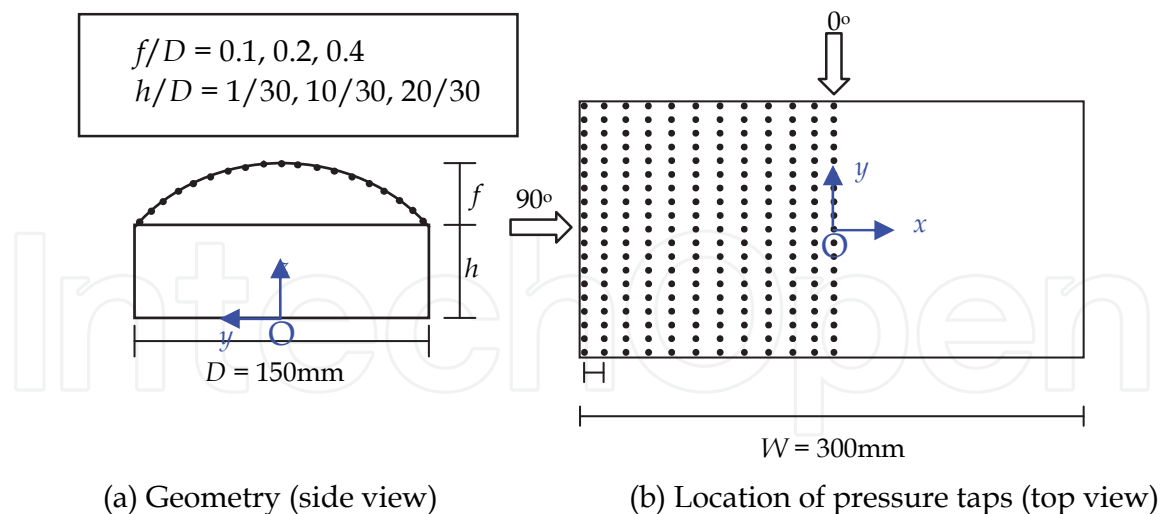


Fig. 3. Wind tunnel model and coordinate system (vaulted roofs)

## 2.2 Database of the statistics of wind pressures

The data from the simultaneous pressure measurements are stored on a computer in the form of pressure coefficient; the pressure coefficient  $C_p$  is defined in terms of the velocity pressure  $q_H (= 1/2\rho U_H^2, \text{ with } \rho \text{ and } U_H \text{ being the air density and the wind velocity at the mean roof height } H, \text{ respectively})$ . Then, the statistical values of pressure coefficients, i.e. mean  $\bar{C}_p$ , standard deviation  $C_p'$ , maximum and minimum peaks,  $C_{p\max}$  and  $C_{p\min}$ , during a full-scale period of 10 min, skewness  $S_k$ , kurtosis  $K_u$  and power spectrum  $S_p(f)$ , with  $f$  being the frequency, are computed. In the spherical dome case, the distributions of  $\bar{C}_p$ ,  $C_p'$ ,  $C_{p\max}$ ,  $C_{p\min}$ ,  $S_k$  and  $K_u$  in the circumferential direction are smoothed by using a cubic spline function. Furthermore, the values at two points that are symmetric with respect to the centreline parallel to the wind direction are replaced by the average of the two values, which makes the distribution symmetric with respect to the centreline. In the case of vaulted roofs, the distributions along the roof's periphery are smoothed by using a cubic spline function. Such a smoothing procedure may eliminate noisy errors included in the experimental data. Sample results on  $\bar{C}_p$  are shown in Figs. 4 and 5. The smoothed data for all the cases tested are stored in the database, together with the coordinates  $(x, y)$  of pressure taps, the values of geometric parameters (i.e.  $f/D$  and  $h/D$ ), and the turbulence intensity  $I_{uH}$  of approach flow at the mean roof height  $H$  and the wind direction (only for vaulted roofs).

The power spectrum  $S_p(f)$  is approximated by the following equation:

$$\frac{S_p(f)}{\sigma_p^2} = a_1 \exp\left(-c_1 \frac{f\sqrt{DH}}{U_H}\right) + a_2 \exp\left(-c_2 \frac{f\sqrt{DH}}{U_H}\right) \quad (1)$$

where  $\sigma_p$  is the standard deviation of pressure fluctuation;  $a_1$  and  $a_2$  are the position constants and  $c_1$  and  $c_2$  are the shape constants. The first and second terms of the right-hand side of Eq. (1) control the position and shape of  $S_p(f)/\sigma_p^2$  at lower and higher frequencies, respectively. Similar representation was used by Kumar and Stathopoulos (1998) for pressures on low building roofs. In the above equation, however, the frequency  $f$  is reduced

by  $\sqrt{DH}$ , not by  $H$ . This is related to a three-dimensional effect of the flow around the roofs. The values of the four constants are determined based on the least squares method applied to the experimental data.

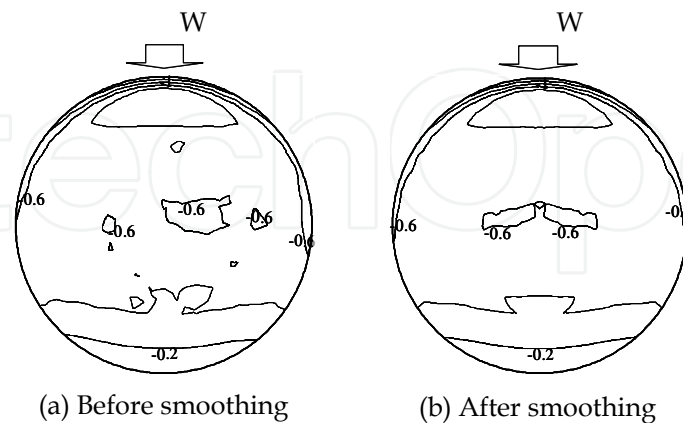


Fig. 4. Distributions of  $\bar{C}_p$  on a spherical dome ( $f/D = 0.1, h/D = 4/16$ , Flow II)

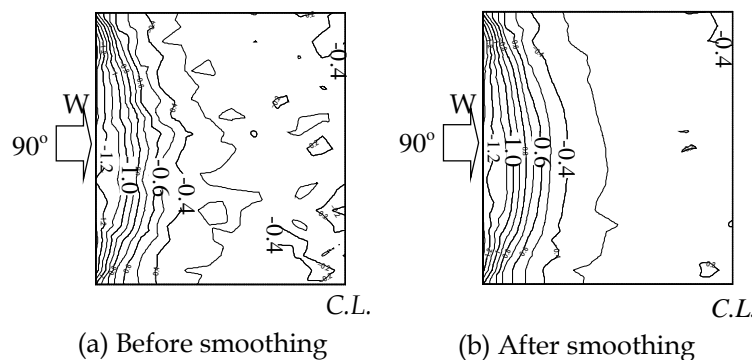


Fig. 5. Distributions of  $\bar{C}_p$  on a vaulted roof ( $f/D = 0.1, h/D = 1/30$ , Flow IV')

In the spherical dome case, the general shape of  $S_p(f)/\sigma_p^2$  changes only slightly in the  $x$ -direction (Noguchi and Uematsu, 2004). Therefore, focus is on the variation of  $S_p(f)/\sigma_p^2$  only in the  $y$ -direction. The values of  $a_1, a_2, c_1$  and  $c_2$  at the pressure taps on the dome's centreline are computed for all the cases tested and stored in the database. In the wind load evaluation system, we use the values of the four constants at a point on the centreline that gives a  $y$ -axis value closest to that of the target point (evaluation point). Fig. 6 shows sample results of comparison between experiment and formula for the power spectra at two points on a spherical dome. The experimental results are plotted by the circles and the empirical formula is represented by the solid line. It is seen that the approximation by Eq. (1) is generally satisfactory.

In the vaulted roof case, the wind pressures are affected by the wind direction. Hence, the power spectra are calculated for all pressure taps and wind directions. Fig. 7 shows sample results of comparison between experiment and formula for the power spectra at two points on a vaulted roof. Again, the agreement is generally good.

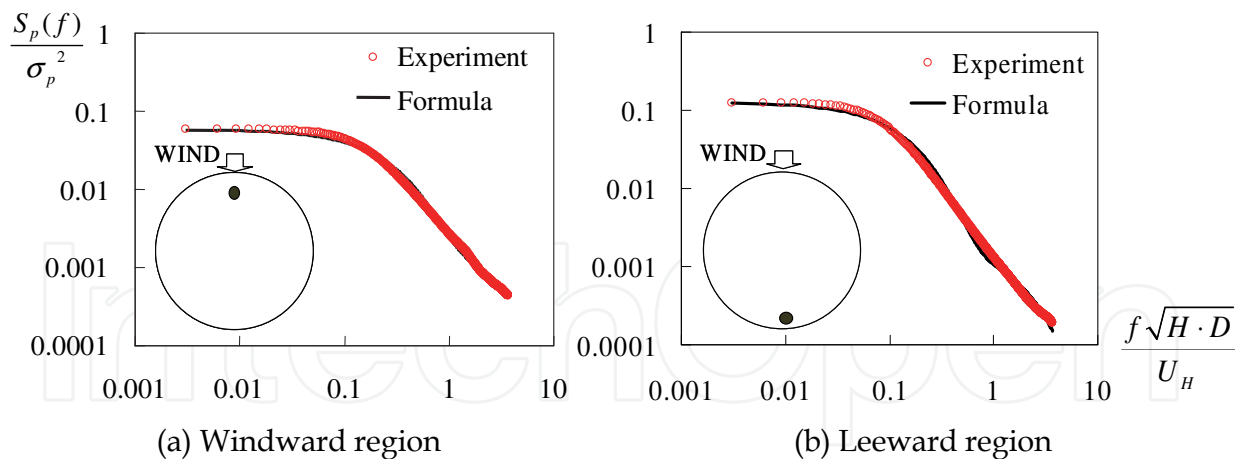


Fig. 6. Wind pressure spectra for a spherical dome ( $f/D = 0.1$ ,  $h/D = 4/16$ , Flow II)

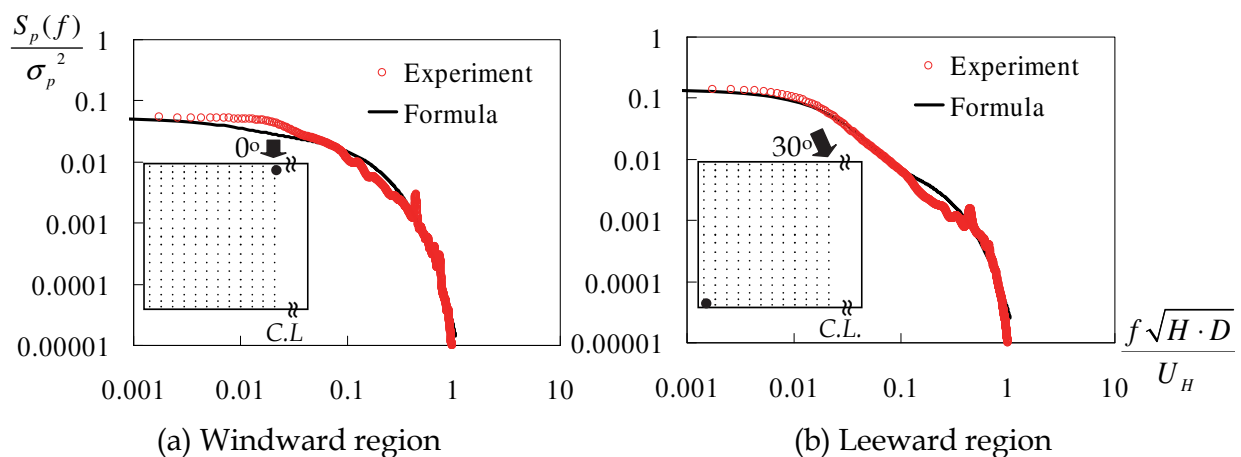


Fig. 7. Wind pressure spectra for a circular arc roof ( $f/D = 0.1$ ,  $h/D = 1/30$ , Flow IV')

### 3. Artificial neural network

#### 3.1 Spherical dome

Although the wind pressures were measured simultaneously at several hundreds points in the wind tunnel experiments, spatial resolution may be still limited from the viewpoint of cladding design. Cladding or roofing cover is sensitive to the spatial variation and fluctuating character of the time-dependent wind pressures. The turbulence of approach flow also affects the wind pressures significantly. Hence, an artificial neural network based on Cascade Correlation Learning Network (CCLN, Fahlman and Lebiere, 1990) is used to improve the resolution.

Fig. 8 illustrates the network architecture, which has a layered structure with an input layer, an output layer and a hidden layer between the input and output layers. The input vector consists of five parameters, that is, two geometric parameters of the building ( $f/D$  and  $h/D$ ), the coordinates ( $x$ ,  $y$ ) of measuring point, and the turbulence intensity  $I_{uH}$  of the approach flow at the mean roof height  $H$ ; the coordinate system is defined as shown in Fig. 2. There is also a bias unit, permanently set to +1. Each network is constructed for each of the four parameters,  $\bar{C}_p$ ,  $C_p'$ ,  $S_k$  and  $K_u$ .

The quickprop algorithm (Fahlman, 1988) is used to train the output weights. Training begins with no hidden units. As the first step, the direct input-output connections are

trained as well as possible over the entire training set. The network is trained until either a predetermined maximum number of iterations is reached, or no significant error reduction has occurred after a certain number of training cycles. If the error is not acceptable after the first step, a new hidden unit is added to the network to reduce this residual error. The new unit is added to the network, its input weights are frozen, and all the output weights are once again trained. This cycle repeats until the error becomes acceptably small.

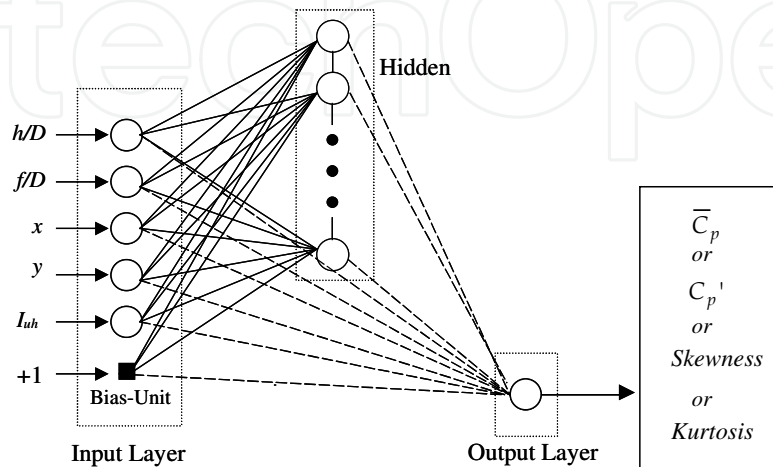


Fig. 8. CCLN for the statistics of wind pressures on spherical domes

Well-distributed representative data are required for training the network. In the above-mentioned database, pressure data at 230 locations are stored each for five  $f/D$  ratios, seventeen  $h/D$  ratios and two kinds of turbulent boundary layers (open-country and urban exposures). Note that the  $h/D$  ratio is varied from 1/16 to 1 in the flat roof case ( $f/D = 0$ ). Therefore, the number of data set is 38,640 ( $= 2 \times (16+17 \times 4) \times 230 = 168 \times 230$ ). Ten typical cases of experimental conditions are selected from these 168 cases. Forty-six locations are randomly selected from the 230 points for testing. Therefore, the number of test data is 460 ( $= 10 \times 46$ ). The other data are used for training the network.

The sigmoid function represented by the following equation is used to process the net input signals and provide the output signals at hidden nodes:

$$f(s) = \frac{S_{\max} - S_{\min}}{1 + e^{-s}} + S_{\min} \quad (2)$$

where  $S_{\max}$  and  $S_{\min}$  represent the upper and lower limits of the output from the neuron. Appropriate values of  $S_{\max}$  and  $S_{\min}$  depend on the output vector. In the training phase of the network using the quickprop algorithm, three empirical terms, i.e. learning rate  $\eta$ , maximum growth factor  $\mu$ , and weight decay term  $\lambda$ , are introduced to improve the convergence of training and the stability of computation. Appropriate values of these terms are determined by trial and error, considering the behaviour of the mean square error that the network produces. The weights are initialised to random numbers between +1.0 and -1.0. The number of epochs also affects the convergence of training, which is again determined by trial and error. Table 1 summarizes the values of  $\eta$  and the numbers of



epochs for  $\bar{C}_p$ ,  $C_p'$ ,  $S_k$  and  $K_u$ , together with the values of the error index  $I_E$  in the training phase; the error index is defined by the following equation:

$$I_E = \frac{\sqrt{\frac{1}{N} \sum_{k=1}^N (T_k - O_k)^2}}{\sigma} \quad (3)$$

where  $T_k$  and  $O_k$  represent the target value and the actual output for training pattern  $k$ , respectively;  $N$  = number of training patterns; and  $\sigma$  = standard deviation of the target data. Because the values of  $S_k$  and  $K_u$  change over a wide range, these values are divided by some factors.

Statistical value	$\eta$	Number of epochs	$I_E$ (training phase)
$\bar{C}_p$	0.5	100	0.144
$C_p'$	0.5	50	0.333
$S_k$	0.02	200	0.478
$K_u$	0.2	300	0.421

Table 1. Characteristics of the neural network for spherical domes

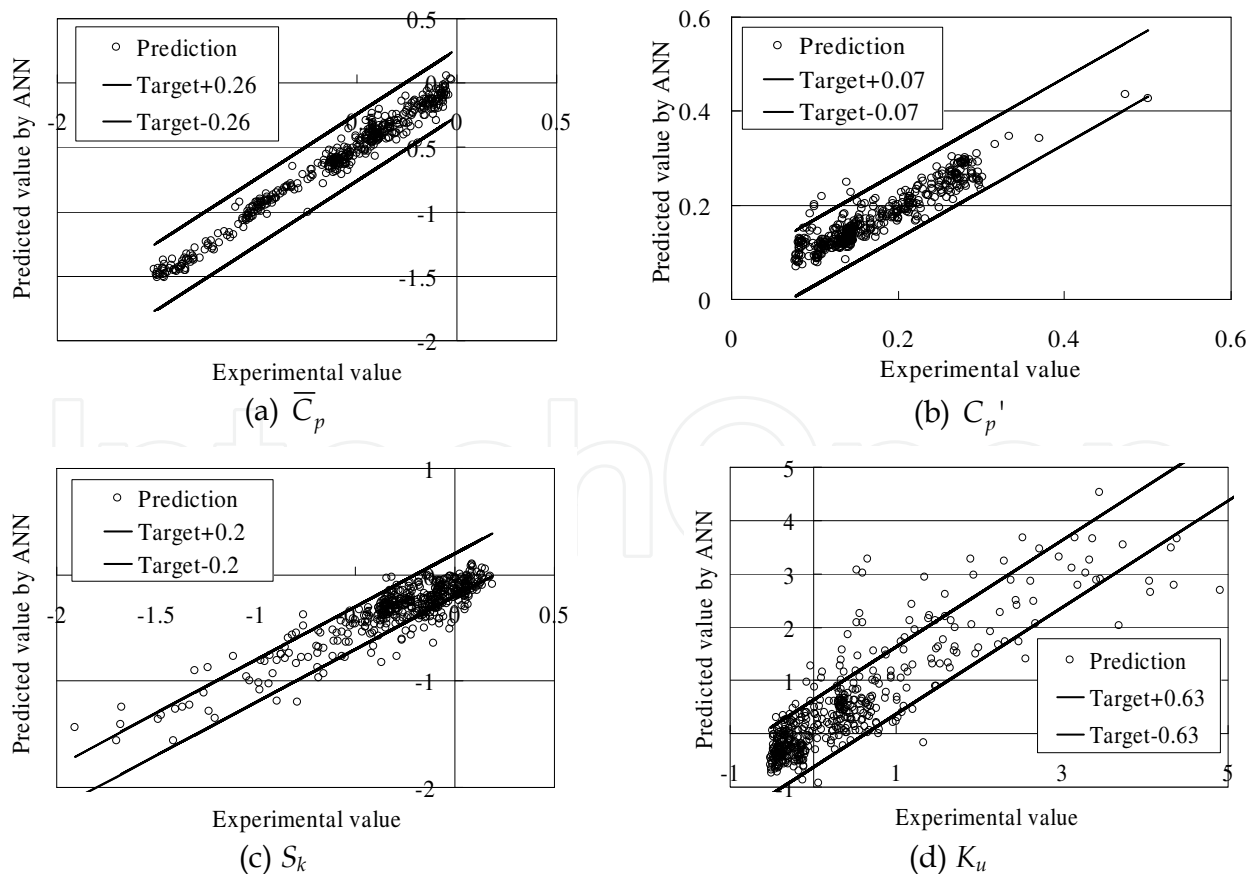


Fig. 9. Comparison between experiment and ANN prediction for  $\bar{C}_p$ ,  $C_p'$ ,  $S_k$  and  $K_u$

Fig. 9 shows comparisons between experiment and prediction by ANN for  $\bar{C}_p$ ,  $C_p'$ ,  $S_k$  and  $K_u$ , respectively; 460 data are plotted in each figure. The solid lines in the figures represent permitted limits, which are tentatively chosen as a standard deviation of the experimental values. Regarding  $\bar{C}_p$  and  $C_p'$ , the agreement is generally good. Regarding the skewness and kurtosis, on the other hand, the agreement is somewhat poorer than that for  $\bar{C}_p$  and  $C_p'$ , although the ANN captures the general trend of the experimental data. This is because the skewness and kurtosis exhibit large values in magnitude in relatively small areas. Furthermore, their variation in these areas is also remarkable. However, as will be described later, the effects of  $S_k$  and  $K_u$  on the simulated time-series of wind pressures are relatively small. This feature implies that the neural networks constructed for  $S_k$  and  $K_u$  can be used in the practical applications.

To discuss the application of the ANN to practical situations, a comparison is made between the prediction by the ANN and the experimental data for Nagoya Dome (Fig. 10). The geometry of this building is as follows: i.e. span  $D = 187.2$  m, rise  $f = 32.95$  m, eaves-height  $h = 30.7$  m ( $f/D = 0.18$ ,  $h/D = 0.16$ ). This dome is constructed in the suburb of Nagoya City, Japan. The wind tunnel experiment was carried out with a 1/500 scale model in a turbulent boundary layer with a power law exponent of  $\alpha = 0.25$  and the turbulence intensity of 0.19 at the level of rooftop. The actual situation in the circular area with a radius of 450 m around the dome was modeled exactly. The experimental data on  $\bar{C}_p$  and  $C_p'$  were provided by Takenaka Corporation that had carried out the wind tunnel experiment. Fig. 11 shows comparisons between the ANN prediction and the experimental data for  $\bar{C}_p$  and  $C_p'$ . The agreement is relatively good, particularly for  $\bar{C}_p$ . The ANN somewhat overestimates the values of  $C_p'$ . However, such a difference up to about 0.1 may be acceptable in practical applications.

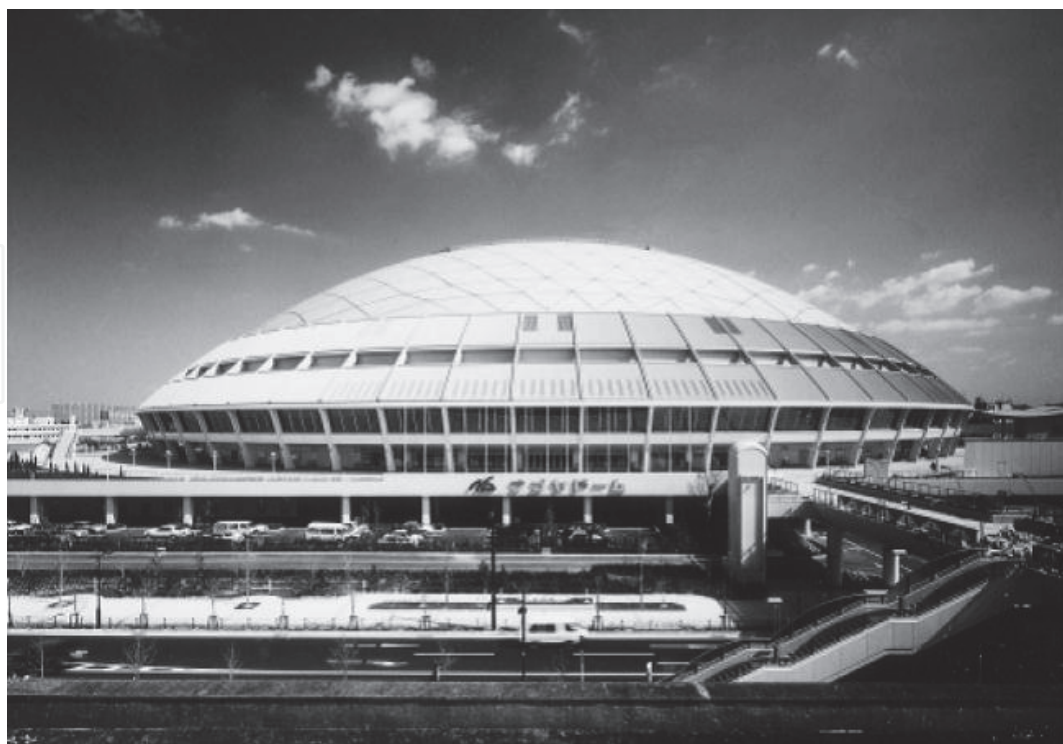


Fig. 10. Nagoya Dome (provided by Takenaka Corporation)

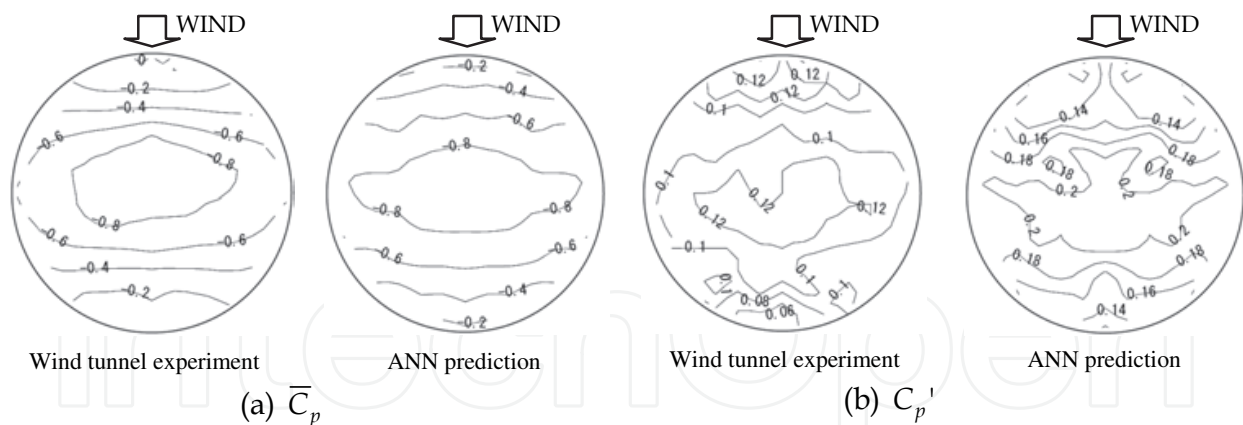


Fig. 11. Comparison between ANN and experiment for the  $\bar{C}_p$  and  $C_p'$  distributions

### 3.2 Vaulted roof

Fig. 12 shows the ANN architecture for vaulted roofs. In this case, the wind direction  $\theta$  is considered in the input vector. The network is trained in the same manner as that for spherical domes. Eighteen typical cases of experimental conditions are selected from the 342 cases. Forty-five locations are randomly selected from the 228 points for testing. The number of test data is 810 (= 18×45). The other data are used for training the network. Table 2 summarizes the characteristics of the network obtained.

Fig. 13 shows comparisons between experiment and prediction by ANN for  $\bar{C}_p$ ,  $C_p'$ ,  $S_k$  and  $K_{uu}$ , respectively; 810 data are plotted in each figure. The behaviour of the networks for vaulted roofs is similar to that for spherical domes shown in Fig. 9. However, the ANN prediction is somewhat poorer than that for spherical domes. This may be related to a wider variation of the characteristics of wind pressures with many parameters in the vaulted roof case.

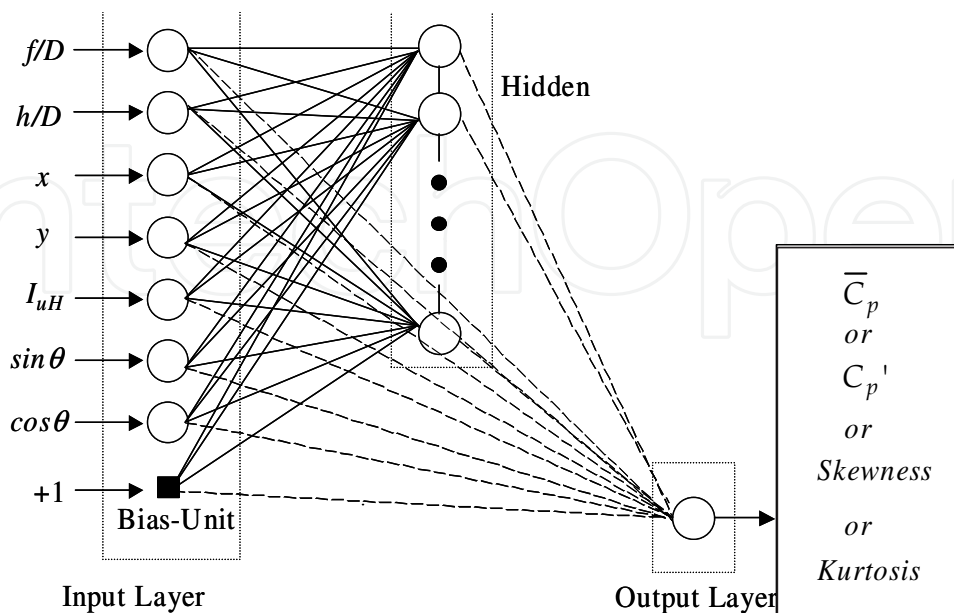


Fig. 12. CCLN for the statistics of wind pressures on vaulted roofs

Statistical value	$\eta$	Number of epochs	$I_E$ (training phase)
$\bar{C}_p$	0.2	150	0.229
$C_p'$	0.5	150	0.378
$S_k$	0.2	300	0.446
$K_u$	0.2	500	0.827

Table 2. Characteristics of the neural network for vaulted roofs

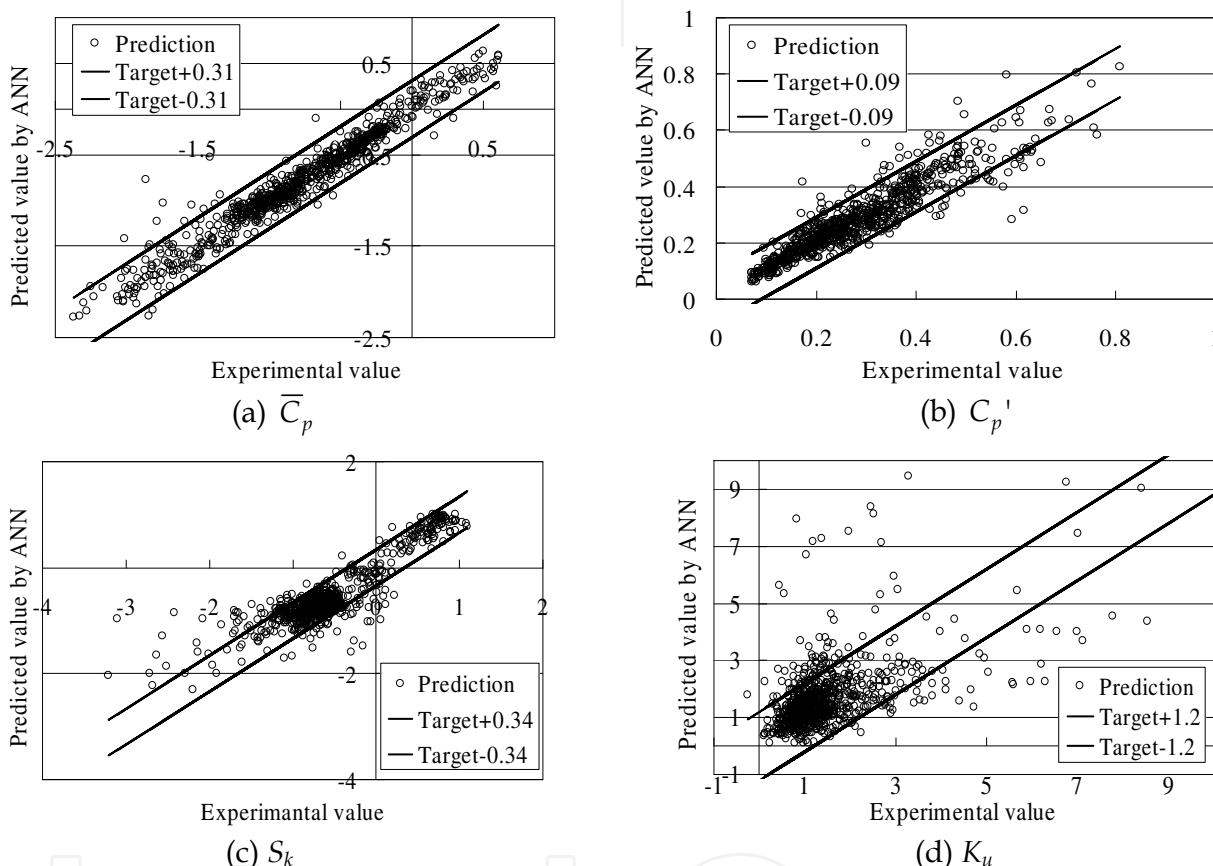


Fig. 13. Comparison between experiment and ANN prediction for  $\bar{C}_p$ ,  $C_p'$ ,  $S_k$  and  $K_u$

#### 4. Time series simulation of wind pressures

##### 4.1 Outline of the procedure

First, the application of the Kumar and Stathopoulos's method (1999, 2001) to the present problem is discussed. The flow chart for the simulation is described in Fig. 14. The approach is based on an FFT Algorithm. The Fourier amplitude is constructed from the power spectrum  $S_p(f)$  of pressure fluctuations, which is represented by Eq. (1). The values of the four coefficients involved in the equation are obtained from the database. The spike features inducing the non-Gaussian character to the pressure fluctuations are achieved by preserving the target skewness and kurtosis given by the ANN and the database. A simple stochastic model with a single parameter  $b$  has been suggested for the simulation of phase. The

computation of  $b$  is accomplished by minimizing the sum of the squared errors in skewness and kurtosis. In practice, changing the value of  $b$  from 0 to 1 with a small increment (e.g. 0.01), the skewness  $S_k$  and kurtosis  $K_u$  of the simulated time series are computed. The sum of the squared errors (SSE) in  $S_k$  and  $K_u$  are calculated for each value of  $b$  and the value giving the least SSE is chosen as the optimum one.

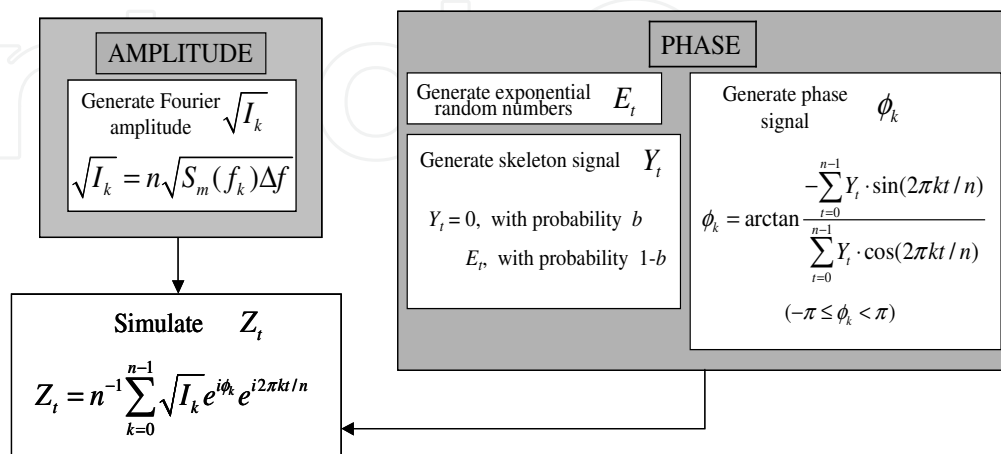


Fig. 14. Schematic of the generation of non-Gaussian wind pressure time series (Kumar and Stathopoulos, 1999, 2001)

#### 4.2 Toward simplification of the procedure

The most troublesome and time-consuming procedure is the determination of the optimum value of  $b$ . Fig. 15 shows sample results on the variation of  $S_k$  and  $K_u$  with  $b$ . Note that the ordinate of the figure for kurtosis is represented by  $K_u-3$ , considering that  $K_u = 3$  for Gaussian processes. Because the skewness and kurtosis are related to each other, both  $S_k$  and  $K_u$  show similar behavior. They increase monotonically with an increase in  $b$ . When the value of  $b$  is relatively small, such as  $b < 0.6$ , for example, the variation is quite small. On the other hand, they increase significantly with increasing  $b$  for larger values of  $b$ . In practice, the optimum value of  $b$  is not so large and the values of  $S_k$  and  $K_u$  are less sensitive to  $b$ . Therefore, the variation of  $S_k$  and  $K_u$  can be approximated by a simple function of  $b$  with a small number of data points in the practical range. The cubic spline function is used here. Using such a function, the optimum value of  $b$  can be calculated easily.

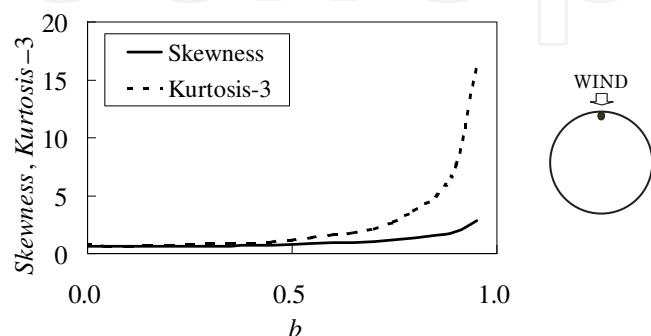


Fig. 15. Variation of  $S_k$  and  $K_u$  with  $b$  for a spherical dome ( $f/D = 0.1$ ,  $h/D = 0.25$ , Flow II)

### 4.3 Results and discussion

A comparison of the wind pressure time series between experiment and simulation is shown in Fig. 16. The spike features of pressure fluctuations are simulated well. Tables 3 and 4 summarize comparisons between experiment and simulation for the statistics of the wind pressures at two typical points on a spherical dome and a vaulted roof, respectively. Note that the averaging time for evaluating the peak pressure coefficients is 1 sec and the values in the table are all the ensemble averages of the results from six consecutive runs. A good agreement between experiment and simulation is seen for both points. Similar comparisons are made for ninety-two points shown in Fig. 17 (points on the solid lines). The results for  $C_{pmax}$  and  $C_{pmin}$  are plotted in Fig. 18. The agreement is relatively good. Approximately 95 % of the simulated results is within a range of the target value  $\pm 0.1$  for  $C_{pmax}$  and  $\pm 0.2$  for  $C_{pmin}$ . These results indicate that the method proposed here can be used for evaluating the design wind loads by combining the database of the statistics of wind pressures and the ANN.

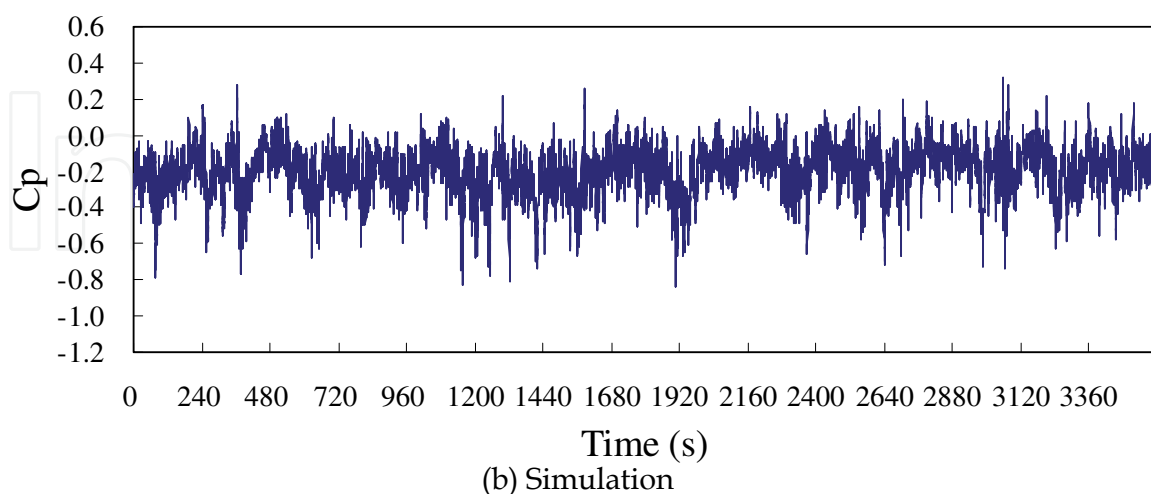
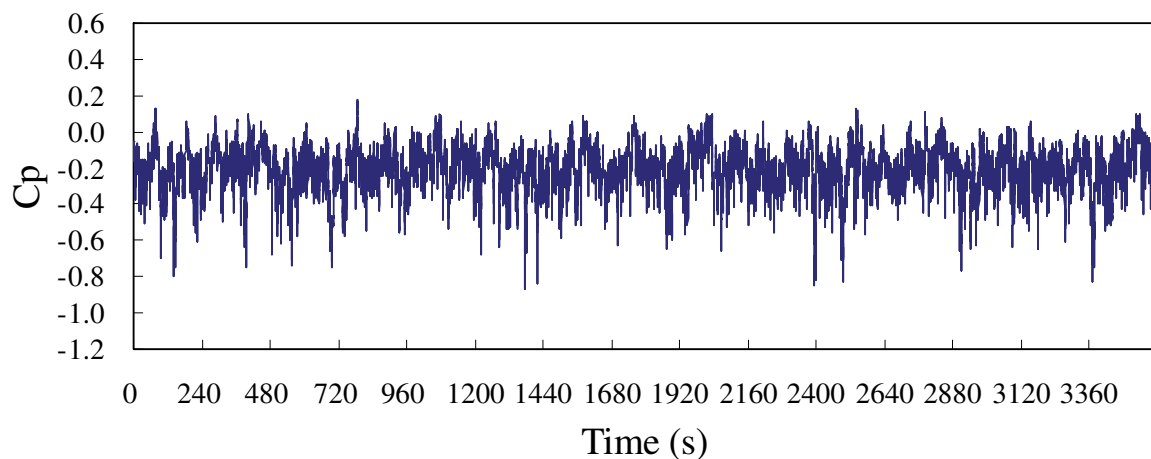


Fig. 16. Experimental and simulated time series of wind pressure coefficient at a point near the leeward edge of a spherical dome ( $f/D = 0.2$ ,  $h/D = 4/16$ , Flow II)

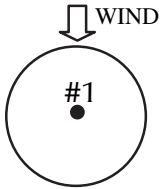
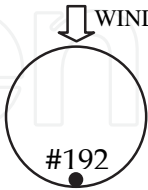
Statistics	$\bar{C}_p$	$C_{pmax}$	$C_{pmin}$	$S_k$	$K_u$	Tap location
(a) Point 1						
Experiment	0.226	-0.394	-1.872	-0.385	3.065	
Simulation	0.211	-0.395	-1.685	-0.436	3.057	
Error	0.015	0.001	-0.187	0.051	0.008	
(b) Point 192						
Experiment	0.126	0.208	-0.742	-0.647	4.225	
Simulation	0.120	0.154	-0.732	-0.661	4.212	
Error	0.006	0.054	-0.010	0.014	0.013	

Table 3. Comparison between experiment and simulation for the statistics of wind pressures on a spherical dome ( $f/D = 0.2$ ,  $h/D = 0.25$ , Flow II)

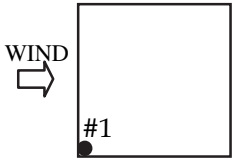
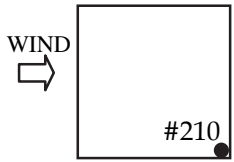
Statistics	$\bar{C}_p$	$C_{pmax}$	$C_{pmin}$	$S_k$	$K_u$	Tap location
(a) Point 1						
Experiment	0.475	-0.437	-3.188	-1.367	3.302	
Simulation	0.437	-0.386	-3.084	-1.188	2.852	
Error	0.038	-0.051	-0.104	-0.179	0.450	
(b) Point 210						
Experiment	0.206	0.115	-1.209	-0.884	2.708	
Simulation	0.190	0.066	-1.142	-0.852	2.332	
Error	0.016	0.049	-0.067	-0.032	0.376	

Table 4. Comparison between experiment and simulation for the statistics of wind pressures on a vaulted roof ( $f/D = 0.3$ ,  $h/D = 10/30$ , Flow II')

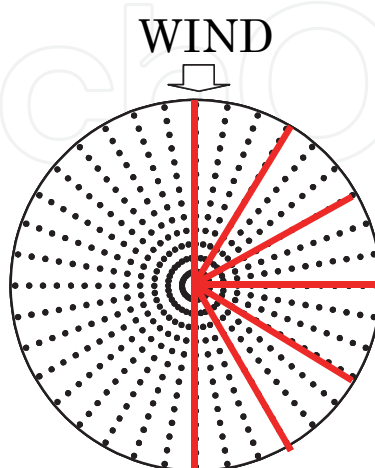


Fig. 17. Tap locations where the time series of pressure fluctuations is simulated (92 points on the solid lines)

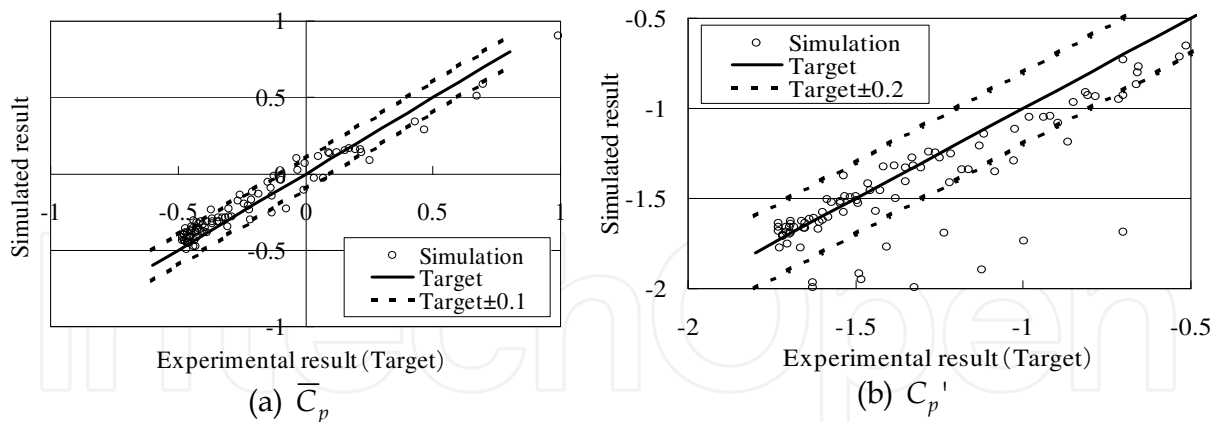


Fig. 18. Comparison between experiment and simulation for a spherical dome ( $f/D = 0.2$ ,  $h/D = 4/16$ , Flow II)

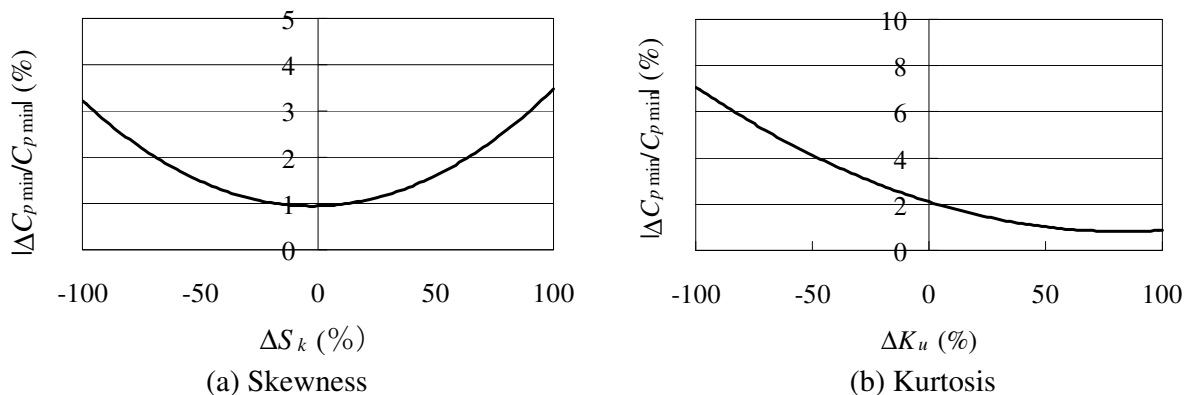


Fig. 19. Effects of  $S_k$  and  $K_u$  on the simulated value of  $C_{pmin}$  for a spherical dome ( $f/D = 0.2$ ,  $h/D = 9/16$ ,  $x/D = 0$ ,  $y/D = -1/4$ )

As mentioned above, the accuracy of the ANN prediction for  $S_k$  and  $K_u$  is not so high, compared with that for  $\bar{C}_p$  and  $C_p'$ . Then, the effects of  $S_k$  and  $K_u$  on the simulated results are investigated. The time series is simulated by changing either  $S_k$  or  $K_u$  from the optimum value. Fig. 19(a) shows the variation of the change of  $C_{pmin}$  ( $\Delta C_{pmin}$ ) with the change of  $S_k$  ( $\Delta S_k$ ) from the optimum value. A similar result for  $K_u$  is shown in Fig. 19(b). It is found that the simulated results are not sensitive to the variation of  $S_k$  and  $K_u$ . In practice, the simulated result of  $C_{pmin}$  changes some 5 percent when the values of  $S_k$  or  $K_u$  change by 50 percent.

### 5. Application of the wind load evaluation system to wind resistant design

The wind load evaluation system proposed here can provide peak pressure coefficients according to a predetermined risk level by combining the extreme value analysis. Fig. 20 shows the probability of non-exceedence for  $C_{pmin}$  at a windward edge point of a spherical dome. The thick solid line shows the result calculated from a set of 200 extremes that the evaluation system predicted. For comparative purpose, the results predicted from 33 sets of six extremes by using BLUE (Lieblein, 1974) are represented by thin solid lines. These results exhibit a considerable scatter around the 200 data curve. The result predicted from



the six experimental data is also quite different from the 200 data curve. Such a difference implies that we need a lot of data for predicting the probability of non-exceedence precisely. It takes a long time to collect so much data in a wind tunnel experiment. By comparison, the proposed wind load evaluation system can provide much data more easily. This is one of the advantages of the system over the wind tunnel experiment.

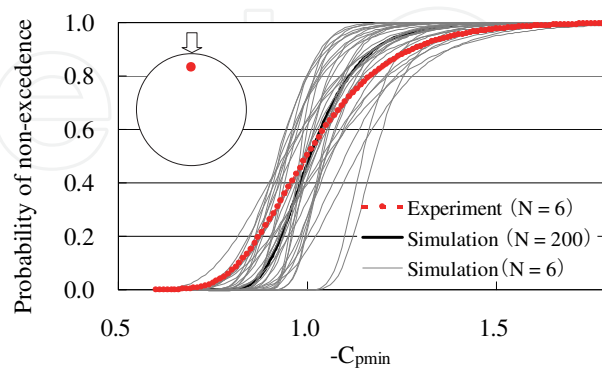


Fig. 20. Probability of non-exceedence for  $C_{pmin}$  (Spherical dome;  $f/D = 0.2$ ,  $h/D = 4/16$ , Flow II)

Furthermore, by introducing a load cycle counting method, such as the rainflow count method, the system can provide the wind load cycles for fatigue design. Fig. 21 shows a sample result on the frequency distribution of wind pressure coefficient fluctuations, represented as a function of mean and amplitude of fluctuation at the center of a dome. By combining such a result with the influence coefficients, we can easily compute the stresses or strains induced in the cladding and its fixings, which are used for evaluating the fatigue damage.

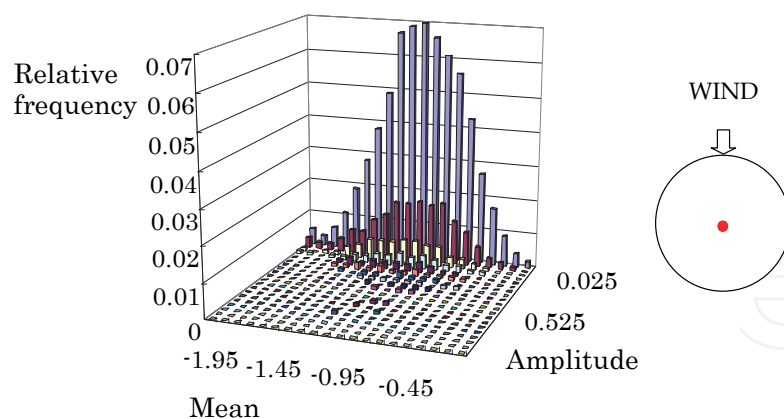


Fig. 21. Number of load cycles (Spherical dome;  $f/D = 0.2$ ,  $h/D = 4/16$ , Flow II)

## 6. Concluding remarks

A computer-assisted load evaluation system for the design of roof cladding of spatial structures using an aerodynamic database, artificial neural network and time-series simulation technique has been proposed. Focus is on spherical domes and vaulted roofs as typical roof shapes used for spatial structures. The proposed methodology is capable of

providing peak pressure coefficients according to pre-determined risk levels by combining the extreme value analysis; this can generate risk consistent and more economical design wind loads for the roof cladding. Furthermore, by introducing a load cycle counting method, such as the rainflow count method, the system can provide the wind load cycles to be used for fatigue design.

This chapter describes the components of the load evaluation system proposed by the author. Although there are some problems to be investigated further, the results presented here indicate that the proposed system is promising. In this chapter the subject is limited to spherical domes and vaulted roofs. However, it is possible to apply the proposed method to the cladding of any buildings, once the database of the statistics of wind pressures has been constructed based on a wind tunnel experiment and/or CFD computations.

## 7. Acknowledgment

A part of the study is financially supported by Nohmura Foundation for Membrane Structure's Technology. The authors are much indebted to Dr. Takeshi Hongo of Kajima Technical Research Institute and Dr. Hirotochi Kikuchi of Shimizu Corporation for providing them the wind tunnel test data. Thanks are also due to Mr. Raku Tsuruishi, Ms. Miki Hamai and Chihiro Sukegawa, who were then graduate students of Tohoku University, for assistance in constructing the neural networks.

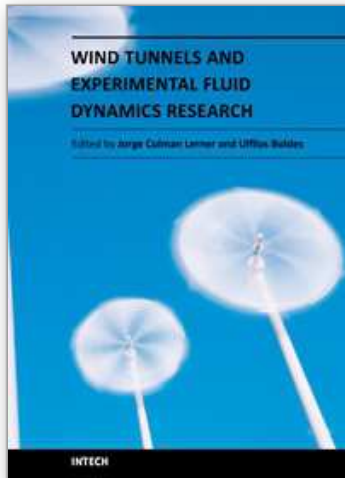
## 8. References

- Fahlman, S.E. (1988). Faster-learning variations on back-propagation: an empirical study, *Proceedings of the 1988 Connectionist Models Summer School*, Morgan Kaufmann.
- Fahlman, S.E. & Lebiere, C. (1990). The cascade-correlation learning architecture, *Advances in Neural Information Processing Systems*, Vol. II, Morgan Kaufmann, pp. 524-532.
- Kumar, K.S. & Stathopoulos, T. (1998). Fatigue analysis of roof cladding under simulated wind loading, *Journal of Wind Engineering and Industrial Aerodynamics*, Vol. 77&78, pp. 171-184.
- Kumar, K.S. & Stathopoulos, T. (1999). Synthesis of non-Gaussian wind pressure time series on low building roofs, *Engineering Structures*, Vol. 21, pp. 1086-1100.
- Kumar, K.S. and Stathopoulos, T. (2001). Generation of local wind pressure coefficients for the design of low building roofs, *Wind and Structures, An International Journal*, Vol. 4, No. 6, pp. 455-468.
- Lieblein, J. (1974). Efficient methods of extreme-value methodology, *National Bureau of Standards*, U.S. Department of Commerce, NBSIR 74-602.
- Nogchi, M.; Uematsu, Y. & Sone, T. (2003). Structural characteristics and wind resistant design of spatial structures constructed in Japan, *Eleventh International Conference on Wind Engineering*, pp. 1595-16002, Lubbock, Texas, USA, June 2-5, 2003.
- Nogchi, M. & Uematsu, Y. (2004). Model of fluctuating wind pressures on spherical domes for load estimation of cladding, *Proceedings of the 18th National Symposium on Wind Engineering*, December 1-3, 2004, Tokyo, Japan, pp. 353-358 (in Japanese).
- Uematsu, Y., Araki, Y., Tsuruishi, R. & Hongo, T. (2005). Wind load evaluation system for cladding of spherical domes using aerodynamic database, neural network and simulation, *Proceedings of the 6th Asia-Pacific Conference on Wind Engineering*, 12-14 September, 2005, Seoul, Korea (CD-ROM).

- Uematsu, Y., Tsuruishi, R., Hongo T. & Kikuchi, K. (2007). A computer-assisted wind load evaluation system for the design of cladding of spatial structures, *Proceedings of the 11th International Conference on Civil, Structural and Environmental Engineering Computing*, 18-21 September, 2007, St. Julians, Malta (CD-ROM).
- Uematsu, Y. & Tsuruishi, R. (2008). Wind load evaluation system for the design of cladding of spatial structures, *Journal of Wind Engineering and Industrial Aerodynamics*, Vol. 96, pp. 2054-2066.

IntechOpen

IntechOpen



## Wind Tunnels and Experimental Fluid Dynamics Research

Edited by Prof. Jorge Colman Lerner

ISBN 978-953-307-623-2

Hard cover, 709 pages

**Publisher** InTech

**Published online** 27, July, 2011

**Published in print edition** July, 2011

The book "Wind Tunnels and Experimental Fluid Dynamics Research" is comprised of 33 chapters divided in five sections. The first 12 chapters discuss wind tunnel facilities and experiments in incompressible flow, while the next seven chapters deal with building dynamics, flow control and fluid mechanics. Third section of the book is dedicated to chapters discussing aerodynamic field measurements and real full scale analysis (chapters 20-22). Chapters in the last two sections deal with turbulent structure analysis (chapters 23-25) and wind tunnels in compressible flow (chapters 26-33). Contributions from a large number of international experts make this publication a highly valuable resource in wind tunnels and fluid dynamics field of research.

### How to reference

In order to correctly reference this scholarly work, feel free to copy and paste the following:

Yasushi Uematsu (2011). A Computer-Assisted Wind Load Evaluation System for the Design of Cladding of Buildings: a Case Study of Spatial Structures, Wind Tunnels and Experimental Fluid Dynamics Research, Prof. Jorge Colman Lerner (Ed.), ISBN: 978-953-307-623-2, InTech, Available from:  
<http://www.intechopen.com/books/wind-tunnels-and-experimental-fluid-dynamics-research/a-computer-assisted-wind-load-evaluation-system-for-the-design-of-cladding-of-buildings-a-case-study>

**INTECH**  
open science | open minds

### InTech Europe

University Campus STeP Ri  
Slavka Krautzeka 83/A  
51000 Rijeka, Croatia  
Phone: +385 (51) 770 447  
Fax: +385 (51) 686 166  
[www.intechopen.com](http://www.intechopen.com)

### InTech China

Unit 405, Office Block, Hotel Equatorial Shanghai  
No.65, Yan An Road (West), Shanghai, 200040, China  
中国上海市延安西路65号上海国际贵都大饭店办公楼405单元  
Phone: +86-21-62489820  
Fax: +86-21-62489821

© 2011 The Author(s). Licensee IntechOpen. This chapter is distributed under the terms of the [Creative Commons Attribution-NonCommercial-ShareAlike-3.0 License](#), which permits use, distribution and reproduction for non-commercial purposes, provided the original is properly cited and derivative works building on this content are distributed under the same license.

IntechOpen

IntechOpen